# Reduction of interior noise in an automobile passenger compartment by means of active structural acoustic control (ASAC)

Malte Misol[1], Stephan Algermissen[2], Hans Peter Monner[3], Anja Naake[4]

[1] German Aerospace Center, 38108 Braunschweig, Germany, Email:malte.misol@dlr.de
[2] German Aerospace Center, 38108 Braunschweig, Germany, Email:stephan.algermissen@dlr.de
[3] German Aerospace Center, 38108 Braunschweig, Germany, Email:hans.monner@dlr.de
[4] Volkswagen AG, 38436 Wolfsburg, Germany, Email:anja.naake@volkswagen.de

## Introduction

The research work presented below deals with the reduction of windshield-vibration-induced interior noise in an automobile passenger compartment by means of active structural acoustic control (ASAC). The investigations are based on former work conducted within the framework of the EU-IP InMAR and make use of an existing test-car equipped with an active windshield [2]. The active windshield consists of the passive structure augmented with optimally placed piezo-ceramic transducers. Main focus of the subsequent work was the development and evaluation of different control strategies (H2, FxLMS) designed with regard to either local or global performance metrics. Due to the lack of a disposable roller test bench, the structural excitation was realized by an electrodynamic exciter (shaker) located at the roof brace between the A-pillars. By this choice it was possible to emulate the structural excitation of the windshield due to rolling and motor force harmonics. In order to achieve a fully structurally integrated sensing and actuation of the windshield vibration the exclusive use of optimally placed piezoelectric transducers was intended. Though, in the experiments, sensing was performed by means of acceleration sensors facilitating a calibration of structural sensor- and laser-scanning vibrometer (LSV) data.

## System

### Control System

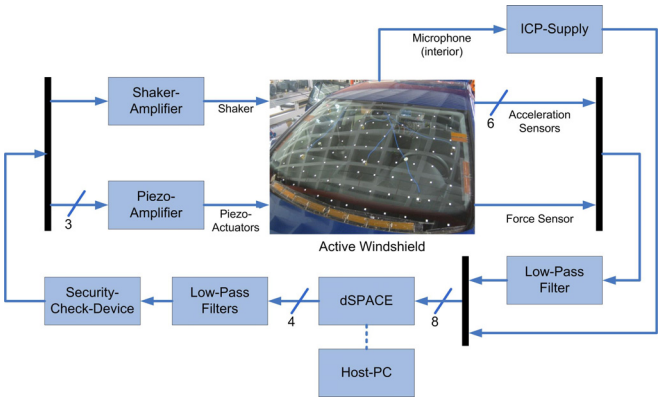


**Figure 1**: Block-Diagram of the control system.

The basic layout of the control system is shown in Figure 1. Kernel of the system is a dSPACE-DS1005 rapid prototyping system. The sampling rate was set to 1 kHz. Apart from the microphone signal, all in- and outgoing signals are conditioned by low-pass filters of type Kemo 21M with a cutoff-frequency set to 240Hz. The piezo-amplifiers of type E-471 and P-270 from PI are sufficiently powerful to supply the piezoelectric $d_{31}$-patches with a maximum voltage of 400V up to the cutoff-frequency. For vibration sensing six accelerometers of type PCB 356A18 are placed at heuristically optimized positions on the windshield. The sound pressure level (SPL) at different positions in the interior is sensed by a PCB 377B02 microphone in combination with a PCB TMS426A01 amplifier. The reference signal for the adaptive feedforward controller was generated from a force sensor placed in the load-path of the shaker near the excitation point at the roof brace.

### Sensors and Actuators

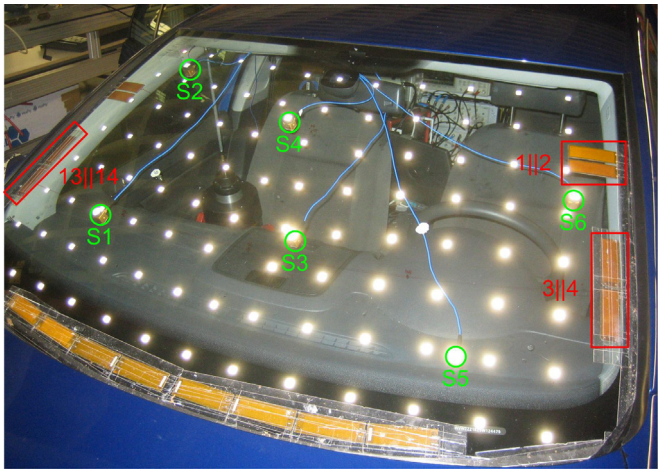


**Figure 2**: Definition of actuators and sensors.

Figure 2 shows the accelerometer positions (S1 to S6) together with the selected piezo-actuators. The number and position of sensors was chosen and optimized heuristically using results from modal analysis of preliminary investigations and the principle of maximum modal observability. The selection-process of the control actuators was guided by the evaluation of control-path frequency-response-functions (FRF). In order to achieve a reasonable trade-off between model complexity and control authority the number of actuator channels was restricted to three. A further increase in control authority was obtained by operating adjacent transducers in parallel. In general, it can be stated that the lower actuators 3,4,13 and 14 have more authority below 150Hz and the upper actuators 1 and 2 perform better above 150Hz. This behavior can be explained by the mode shapes of the windshield-system and the corresponding distribution of maximum modal strains. The final choice of actuators was 1||2, 3||4 and 13||14 because in this configuration the singular values of the control path FRF-matrix are largest throughout the controller bandwidth.

### System Identification

For the design and implementation of a feedback- or feed-forward controller a suitable system model is needed. Here the slicot-toolbox [6] was used to calculate a time-discrete state-space-model for the coarse accelerometer grid (4 Inputs, 6 outputs) from multiple-reference test data. In order to obtain the global system-dynamics in terms of a fine, so-called LSV-grid (101 points), a subsequent least-squares fit was performed using the obtained state-space model and measurement data from the laser-scanning vibrometer. The final result was an augmented state-space system of the same order but with 101 outputs. Figure 3 compares the singular values of the identified system model with measurement data. Hence, with the use of only 60 states a numerically efficient and accurate modeling of the 404 transfer paths was achieved.

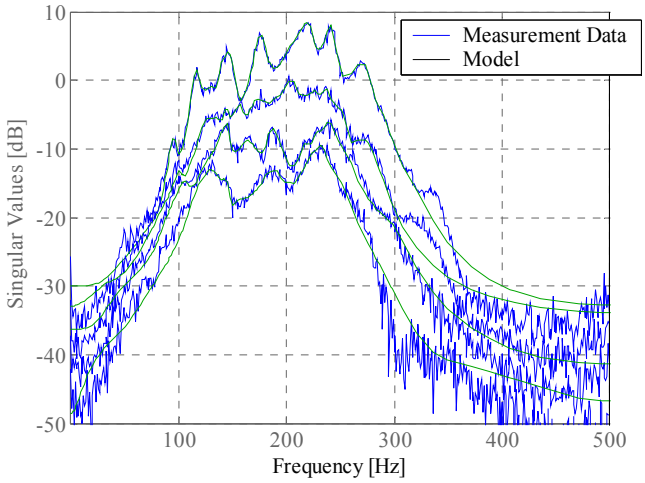


**Figure 3** Singular values of control- and disturbance path FRF-matrix.

## Control

Modern control strategies are based on the concept of a generalized plant [4]. This method is very generic and provides great flexibility in control strategy formulation. The overarching concept of most control design concepts is reflected by the minimization of a well-defined performance metric described in terms of a matrix-norm (e.g. $H_2$ or $H_\infty$).

For reasons of brevity the subsequent discussion of the experimental results is restricted to the second and third eigenfrequency of the windshield-system. The relevance of these two vibration modes for low-frequency interior noise has been proven in preliminary acoustic investigations conducted by the industry partner Volkswagen AG.

In order to allow comparability, the color coding of the vibration amplitudes shown in Figure 4 was kept constant for all LSV-measurements.

During the experiments it was observed, that the shaker-excitation prevents the occurrence of normal modes in the measured operational deflection shapes (ODF). This fact in combination with the small number of independent actuator-channels was considered as a limiting factor on control-performance especially at higher frequencies.

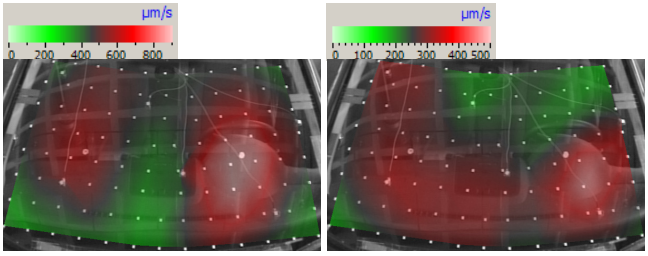


**Figure 4** Measured ODF at 116Hz (left) and 145Hz (right) without control.

### State-Feedback Control ($H_2$)

Figure 5 shows the schematic which was employed for the control design. This formulation follows the generalized plant concept with plant G, controller R and appropriately chosen weighting filters W. The zero-mean, white-noise processes $w_d$ and $w_r$ serve as inputs (process- and measurement noise) whereas z represents the performance output of the generalized plant.

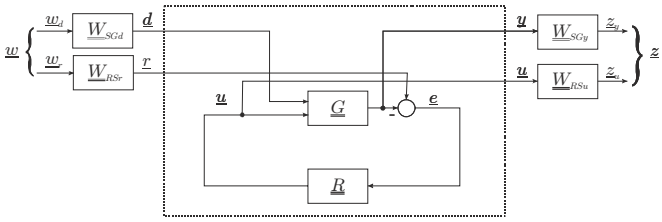


**Figure 5** Control-Scheme with weightings and controller.

With the definition of sensitivity S and complementary sensitivity T according to (1) the scheme can be expressed mathematically as (2). The desired minimization of the performance-output power for a random input can be equivalently formulated as minimizing the $H_2$-Norm of the transfer function $T_{zw}$ from w to z.

$$\underline{\underline{S}} = \left[\underline{\underline{E}} + \underline{\underline{G}}\,\underline{\underline{R}}\right]^{-1} \qquad (1)$$
$$\underline{\underline{T}} = \underline{\underline{G}}\,\underline{\underline{R}}\,\underline{\underline{S}}$$

$$\begin{bmatrix} \underline{z}_y \\ \underline{z}_u \end{bmatrix} = \begin{bmatrix} \underline{\underline{W}}_{SGy}\,\underline{\underline{T}}\,\underline{\underline{W}}_{RSr} & \underline{\underline{W}}_{SGy}\,\underline{\underline{SGW}}_{SGd} \\ \underline{\underline{W}}_{RSu}\,\underline{\underline{RSW}}_{RSr} & -\underline{\underline{W}}_{RSu}\,\underline{\underline{RSGW}}_{SGd} \end{bmatrix} \begin{bmatrix} \underline{w}_r \\ \underline{w}_d \end{bmatrix} \qquad (2)$$

In order to achieve the maximum possible control performance, a model of the disturbance path was included into the generalized plant. This forces the control design process to put more emphasis on frequency bands with a high disturbance excitation level and furthermore permits an accurate numerical prediction of control performance. Of course, disturbance path modeling is not always possible in real systems with complex excitation. Then a fictitious injection of disturbance must be assumed for the control design algorithm.

The comparison of Figures 6 and 7 suggests that the performance of the two different controllers is relatively similar even though the globally optimized controller works slightly better. As expected it achieves a more homogenous reduction in vibration amplitude. Furthermore the fine LSV-grid opens up the possibility of a sound power estimation based

on structural sensor information. The drawback of this method clearly lies in the necessity to alter the control system structure during system identification preventing an online updating of the control path dynamics.

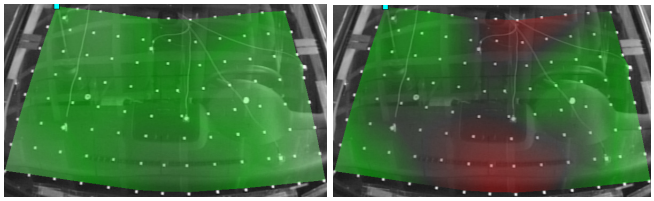

**Figure 6** Measured ODF at 116Hz (left) and 145Hz (right) with $H_2$-Controller designed for the coarse sensor-grid.

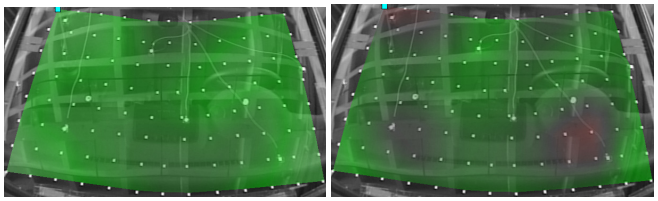

**Figure 7** Measured ODF at 116Hz (left) and 145Hz (right) with $H_2$-Controller designed for the fine LSV-grid.

### Adaptive Feedforward Control (FxLMS)

The applicability of adaptive feedforward control depends on the existence of a reference signal that is sufficiently time advanced and highly correlated with the sensor-signals. If these severe constraints are fulfilled, a very powerful and robust control system can be designed. Robustness comes from the fact that the FIR-filters are non-recursive and hence have no poles. Apart from actuator to reference-sensor feedback, the only source of potential instability lies in the filter-weight adaptation process which diverges if the phase differences between modeled and real plant dynamics exceed ±90°. In contrast to the observer-based state-feedback control scheme, the implemented MIMO-FxLMS performs no post-processing of the sensor signals and hence can only process local information based on the coarse sensor-grid (z ≡ e). For this reason the measured ODF resemble the ones depicted in Figure 6.

Adaptive filtering was performed with 200 FIR-filter taps for each control channel, a leakage-factor ν = 1 and a normalized step size μ of 0.1% times the theoretical maximum value.

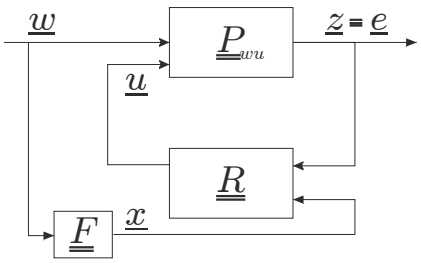


**Figure 8** Generalized plant framework for the adaptive feedforward controller (FxLMS)

According to [3] the adaption process of the filter-weights for a single-reference MIMO-FxLMS with M sensors and K actuators is described by (3).

$$\underline{w}(n+1) = \underline{w}(n) + \mu \underline{\underline{X}}'(n)\underline{e}(n) \quad (3)$$

The dimensions of weight-vector w, filtered-reference matrix X' and error-vector e follow from (4). Matrix X' is formed by the Kronecker product convolution of impulse response matrix S and reference signal vector x.

$$\underline{w}(n) \equiv \left[\underline{w}_1^T(n) \quad \underline{w}_2^T(n) \quad \cdots \quad \underline{w}_K^T(n)\right]^T \in \mathbb{R}^{KL}$$

$$\underline{e}(n) \equiv \left[e_1(n) \quad e_2(n) \quad \cdots \quad e_M(n)\right]^T \in \mathbb{R}^{M} \quad (4)$$

$$\underline{\underline{X}}'(n) = \hat{\underline{\underline{S}}}^T(n) \otimes \underline{x}(n) \in \mathbb{R}^{KLxM}$$

The SPL shown in Figures 9 and 10 were measured at six arbitrarily chosen points about 0.1m away from the inner surface of the windshield. These results are intended to give a first impression of the sound reduction potential that opens up with the application of active methods. The realization of profound intensity- or sound power measurements was beyond the scope of these investigations and remains as a topic of further investigations.

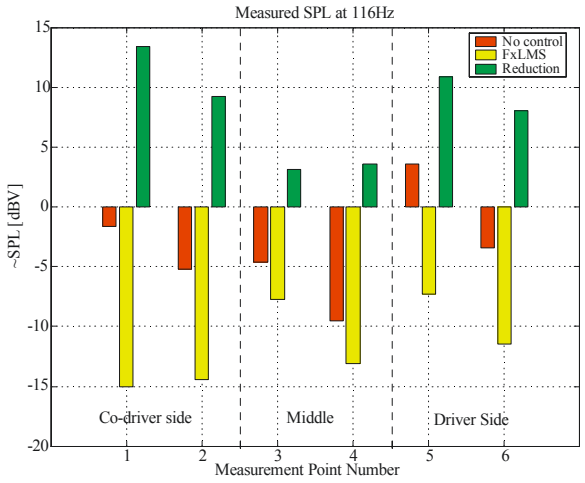


**Figure 9** Reduction in SPL at 116Hz achieved by the adaptive feedforward controller (FxLMS)

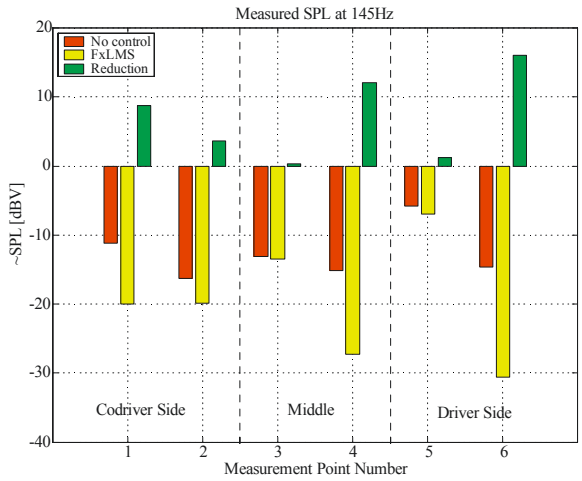


**Figure 10** Reduction in SPL at 145Hz achieved by the adaptive feedforward controller (FxLMS)

## Conclusion

In this work different control strategies for the active reduction of windshield-vibration-induced interior noise have been developed and experimentally approved. The comparison of vibration level in open- and closed loop showed a global reduction of 5dB to 7dB in the acoustically relevant frequency band containing the second and third eigenmode of the windshield-system (100Hz to 150Hz). The acoustic effects, although not profoundly scrutinized within the scope of this work, are reflected in a reduction up to 15dB in SPL.

These promising results may encourage future work on this topic. Possible questions for subsequent research activities concern the implementation of piezoelectric transducers for a structurally integrated sensing and the use of a larger number of low-voltage piezo-actuators in order to handle the observed complex operational deflection shapes. Also a further development of sound power estimation based on structural information or a frequency-selective post-processing of sensor data might be in the focus of prospective research activities.

## Literature

[1] Algermissen, S., Keimer, R., Rose, M. and Monner, H. P.: Robust Control for Vibration Suppression on Parallel Robot TRIGLIDE. Proc. of Adaptronic Congress (2006)

[2] Naake, A., Schmidt, K. and Meschke, J.: Vehicle Windshield with Active Noise Reduction. Proc. of Adaptronic Congress (2007)

[3] Kuo, S. M., Morgan, D. R.: Active Noise Control Systems: Algorithms and DSP Implementations. Wiley, New York, 1996

[4] Clark, R. L., Saunders, W. R., Gibbs, G. P.: Adaptive Structures. Wiley, New York, 1998

[5] Zhou, K.: Essentials of Robust Control. Prentice Hall, 1998

[6] Favoreel, W., Sima, V., Van Huffel, S., Verhaegen, M. and De Moor, B.: SLICOT Working Note 1998-6: Subspace Model Identification of Linear Systems in SLICOT, Technical report, European Community BRITE-EURAM III Thematic Networks Programme NICONET.